Supporting Information

Photocatalytic fixation of nitrogen to ammonia with Ce/S co-doped TiO_2 catalyst: Synergistic tuning of heterovalent metal states and oxygen vacancy defects

Pengkun Zhang[1], Longyan Chen[1], Dong-Hau Kuo[2,*], Binghong Wu[1], Zhengjie Su[1], Dongfang Lu[1,*], Qinhan Wu[1], Jiqing Li[1,*], Jinguo Lin[1,*], Xiaoyun Chen[1,*]

[1] College of Materials Engineering, Fujian Agriculture and Forestry University, Fuzhou 350002, China

[2] Department of Materials Science and Engineering & Graduate Institute of Energy and Sustainability Technology, National Taiwan University of Science and Technology, Taipei 10607, Taiwan

*Corresponding author

E-mail address: dhkuo@mail.ntust.edu.tw (D. H. Kuo)

E-mail address: fjldf@126.com (D. Lu)

E-mail address: nfuljq@163.com (J. Li)

E-mail address: fjlinjg@126.com (J. Lin)

E-mail address: fjchenxy@126.com (X. Chen)

Experimental Section

1. *Computation of apparent quantum efficiency (AQE) and solar-to-ammonia (STA) conversion efficiency*

According to the literature reports [1], the apparent quantum efficiency (AQE) is determined. The catalytic experiments for determining AQE were performed in pure water (100 mL) without any sacrificial reagents. 50 mg of TiCeOS-3, used as the photocatalyst, was added to the solution. A 300 W Xe lamp irradiated the reaction solution with a band-pass filter for the wavelength of 420 nm. A CEL-NP2000 photoradiometer measured the photon flux of the incident light. The AQE is calculated according to the equation below:

$$\text{AQE}=\frac{\text{Number of reacted electrons}}{\text{Number of incident photons}}\times 100\%=\frac{6\cdot n_{AM}\cdot N_A}{\frac{W\cdot A\cdot t}{h\cdot v}}\times 100\%$$

where n_{AM} represents the molar number of generated ammonia, while W, A, t, and ν are for the incident light intensity, irradiation area, time, and frequency, respectively. N_A and h are Avogadro's constant and Planck constant, respectively.

According to the literature reports [2, 3], to determine the Solar-to-Ammonia (STA) conversion efficiency, reactions were performed using a solar simulator, where the efficiency was calculated as STA = [ΔG for NH_3 generation ($J\cdot mol^{-1}$)] × [NH_3 evolved (mol)] [total input energy (W)] × [reaction time (s)] × 100% In the above equations, the ΔG° values for NH_3 generation is 339 $J\cdot mol^{-1}$. The overall irradiance of the AM1.5G spectrum was 100 mW cm^{-2}, and the irradiation area was 4.26 cm^2.

$$STA=\frac{[\Delta G \text{ for } NH_3 \text{ generation } (J\cdot mol^{-1})]\times[NH_3 \text{ evolved (mol)}]}{[\text{total input energy (W)}]\times[\text{reaction time (s)}]}\times 100\%$$

In the above equations, the ΔG° values for NH_3 generation is 339 $kJ\cdot mol^{-1}$. The overall irradiance of the AM1.5G spectrum was 100 mW cm^{-2}, and the irradiation area was 4.26 cm^2.

2. NH_3 product characterization and qualification.

2.1 Indophenol blue method

The concentration of ammonium ions was determined via the indophenol blue method [4, 5]. The mixed solution at the end of the photocatalytic reaction was centrifuged and filtered with a 0.02 μm PTFE (polytetrafluoroethylene) membrane, then 4 mL of the mixture solution was removed in a colorimetric tube and 2 mL of 1M NaOH solution (containing 5 wt% salicylic acid, 5 wt% sodium citrate) were added, followed by 1 mL of 0.05 M NaClO and 0.2 mL of 1 wt% sodium nitroprusside solution each. After mixing all the reagents, a yellow-green solution was obtained. The mixture solution was reacted for 2 h under light-protected conditions, and the absorbance at λ= 688 nm was recorded via a TU-1901 ultraviolet-visible spectrophotometer. According to the Lambert-Beer's Law calculation, the NH^{4+} concentration.

2.2 Nessler's reagent method

The concentration of ammonium ions was determined via the Nessler reagent method [6, 7]. The supernatant was centrifuged individually at the end of the reaction and filtered with a 0.02 μm PTFE (polytetrafluoroethylene) membrane and then placed into a 10 mL colorimeter tube, to which 0.2 mL of potassium sodium tartrate solution and Nessler's reagent was added, shaken well, and then left to stand for 10 min. Finally, the concentration of NH^{4+} was measured at 420 nm via a TU-1901

ultraviolet-visible spectrophotometer. The concentration of NH^{4+} was calculated via the Lambert-Beer's Law.

2.3 Watt-Chrisp method conditions

The concentration of ammonium ions was determined via the Watt-Chrisp method [8]. Mix 2 g of (dimethylamino) benzaldehyde with 10 mL of concentrated solution, HCl, and 100 mL of ethanol, and use it as a reagent for the determination of hydrazine. Then, take 1 mL of the reagent and add the mixture to the remaining 1 mL of the reaction mixture. After 30 min, measure the absorption of the solution at 455nm using a UV visible spectrometer.

2.4 Ion chromatography test conditions

According to the literature reports [9], The Thermo Fisher ICS-600 cationic ion chromatograph with Pac CS12 A 4×250 mm (ICS) was further used to determine the NH_3 concentration. The testing conditions are listed in Table S1.

Table S1 ICS determines the conditions of the NH_3 concentration

Conditions	Details	Conditions	Details
Analytical column	Ion Pac CS12 A 4×250 mm	Run time	15 min
Protective column	Ion Pac CG12A 4×50 mm	Detector	Conductivity detector
Leachate	20 mM Methyl sulfonic acid aqueous solution	Suppressor	CDRS 600 (4 mm) Self-circulation inhibition
Flow rate	1.0 mL/min	Sample injector	AS-DV
Sample volume	10 ul	Sampling mode	Automatic sampling

Additional figures and tables

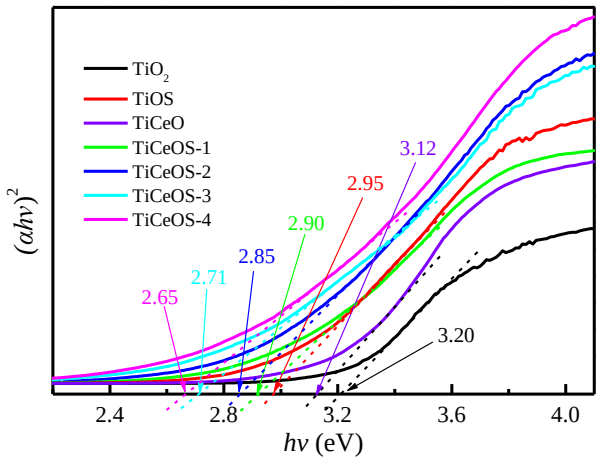

Fig. S1 The ultraviolet-visible absorption spectra of TiO_2, TiOS, TiCeO, and TiCeOS catalysts converted to the $(\alpha h\nu)^2$-$h\nu$ plots for the direct bandgap calculation.

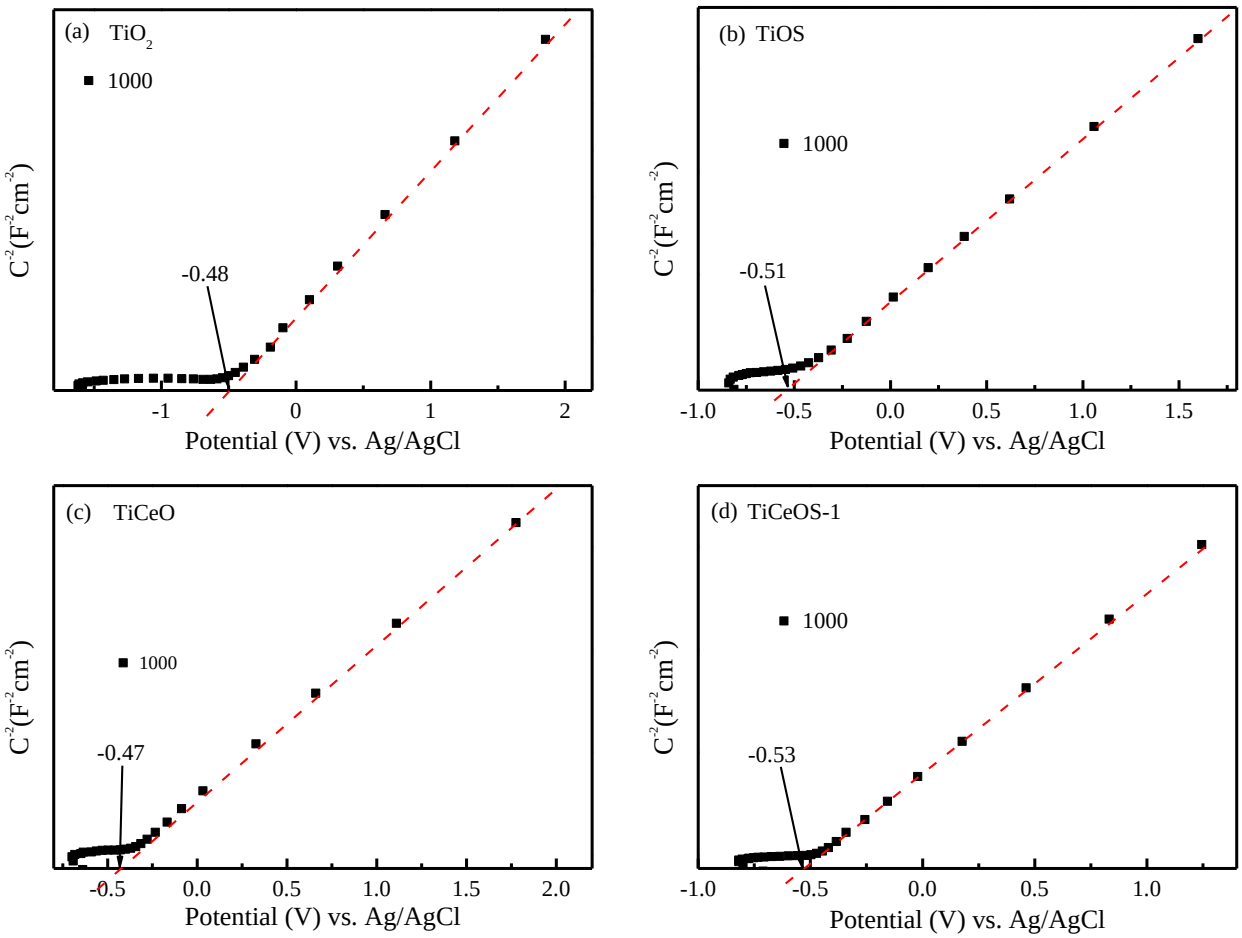

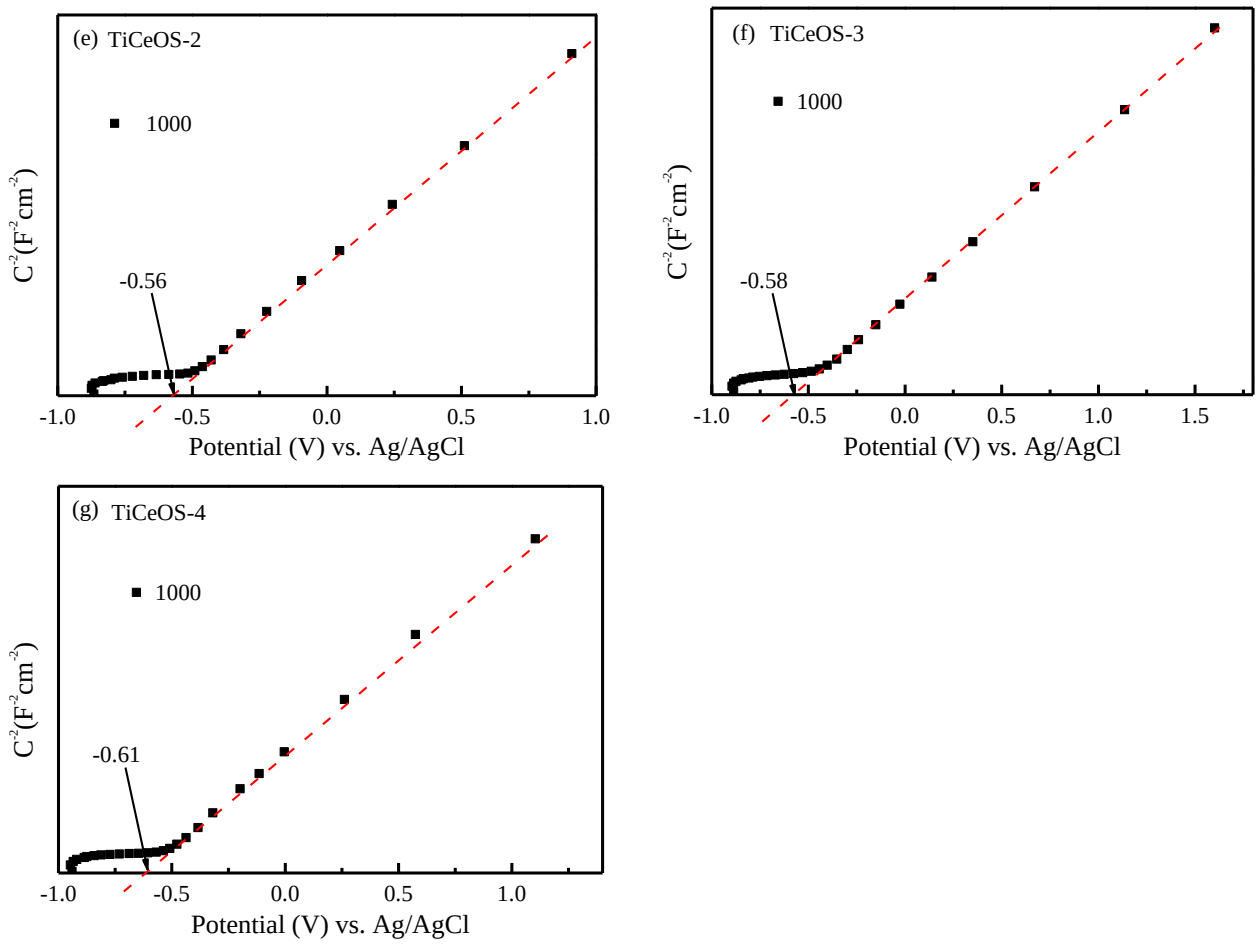

Fig. S2 (a-g) Mott–Schottky curves of TiO_2, TiOS, TiCeO, and TiCeOS conducting at 1000 Hz.

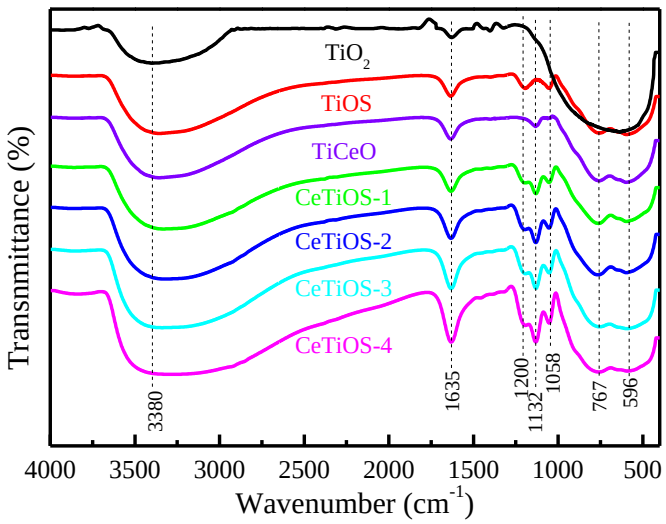

Fig. S3 FTIR spectra of TiO_2, TiOS, and TiCeOS catalysts.

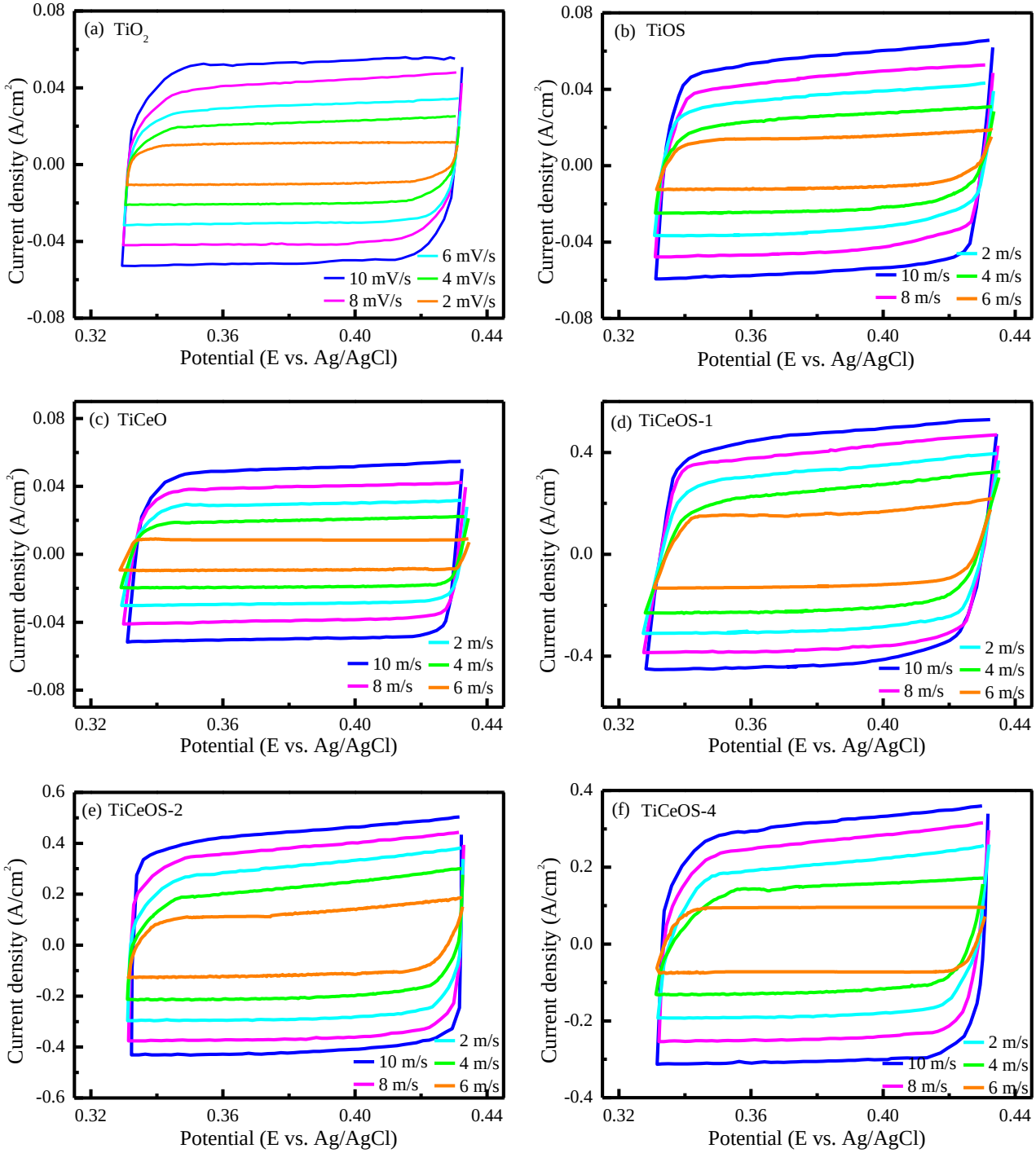

Fig. S4 CV curves of TiO_2, TiOS, TiCeO, and TiCeOS catalysts.

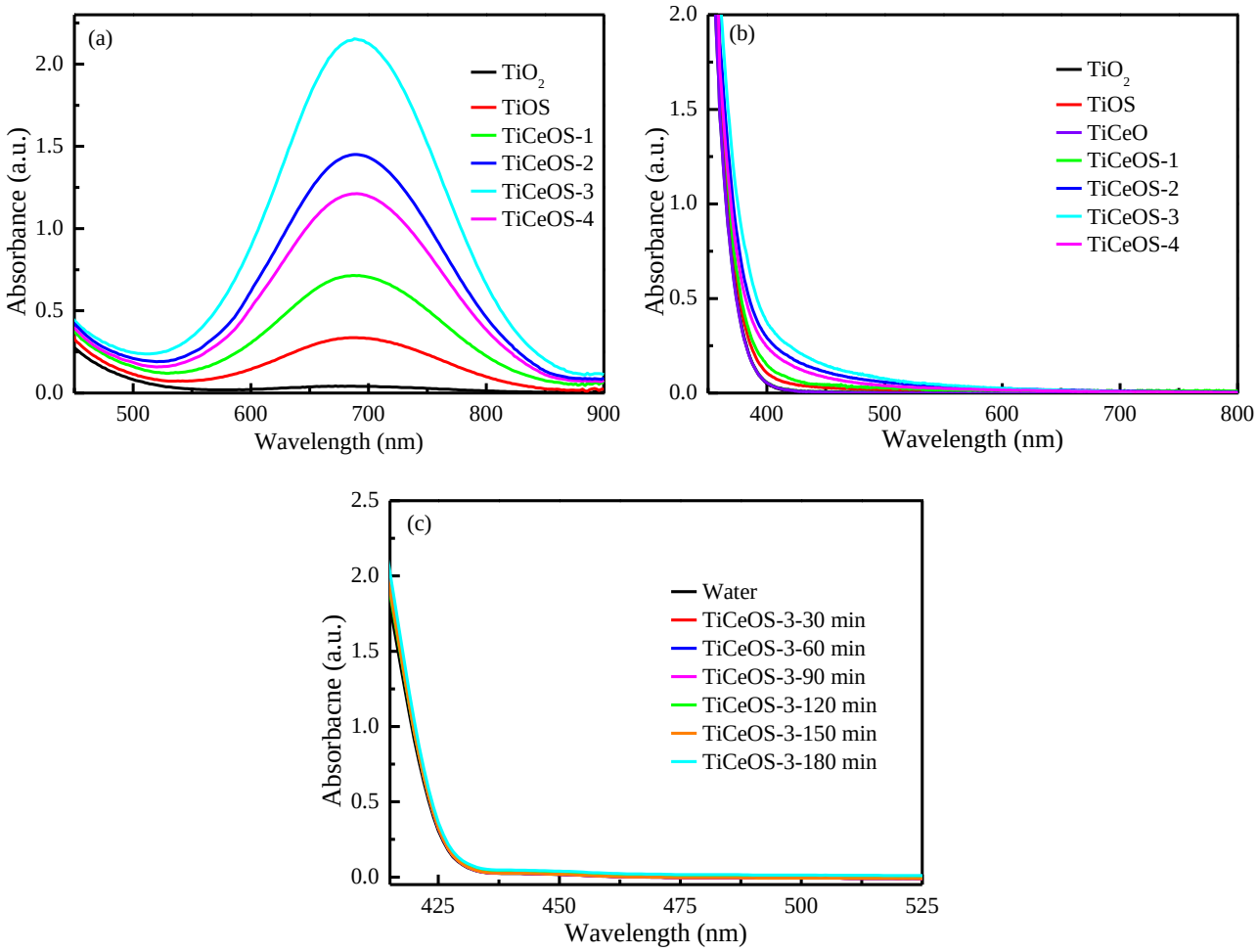

Fig. S5 The test results of (a) indophenol blue, (b) Nessler's reagent, and (c) Watt-Chrisp methods.

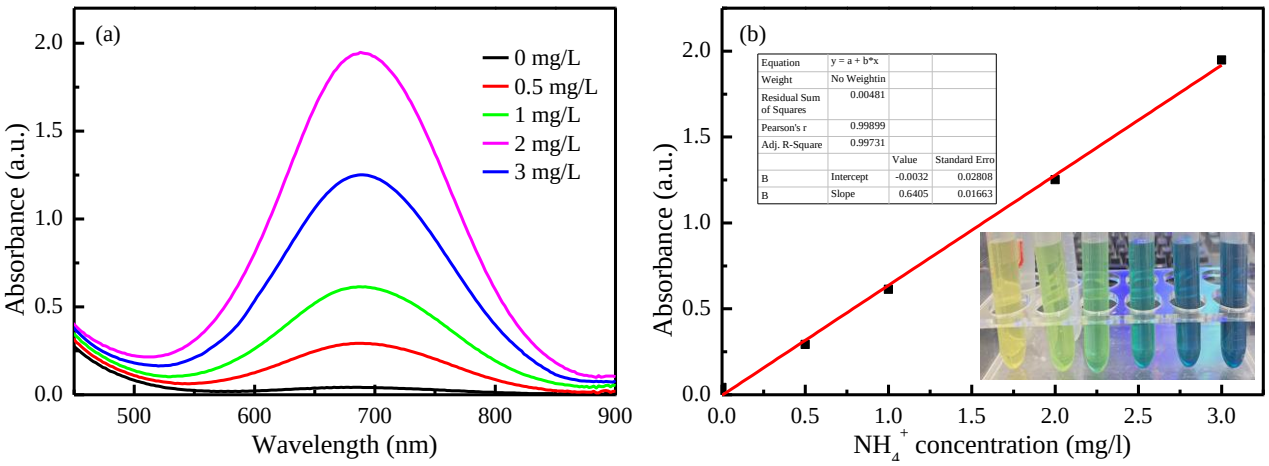

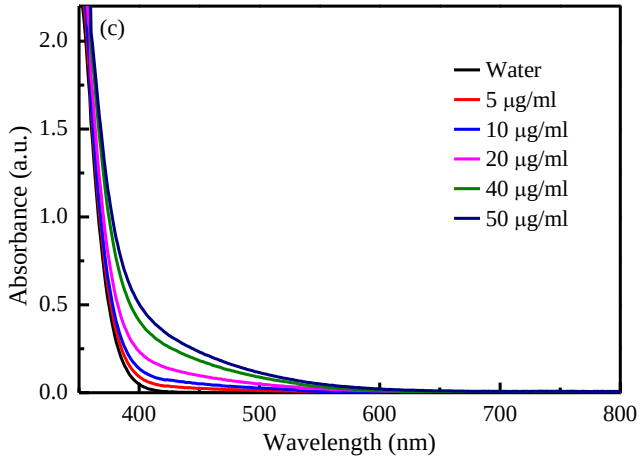

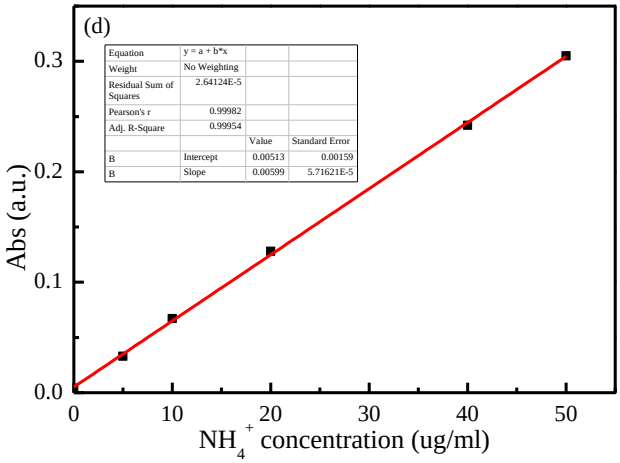

(e)

Injection Name	Ret.Time min ECD_1	Area μS*min ECD_1	Height μS ECD_1	Amount ECD_1
	NH4+	NH4+	NH4+	NH4+
0.5	4.757	0.0615	0.409	0.273
1	4.764	0.1184	0.772	0.920
2	4.767	0.2203	1.402	2.104
5	4.781	0.4793	2.851	5.279
10	4.774	0.8392	4.753	10.197
20	4.787	1.3800	7.448	19.439
30	4.787	1.7911	9.359	30.373
40	4.797	2.1545	11.008	n.a.
50	4.807	2.5703	12.926	n.a.
Average	4.780			
Rel. Std. Dev.	0.341 %			

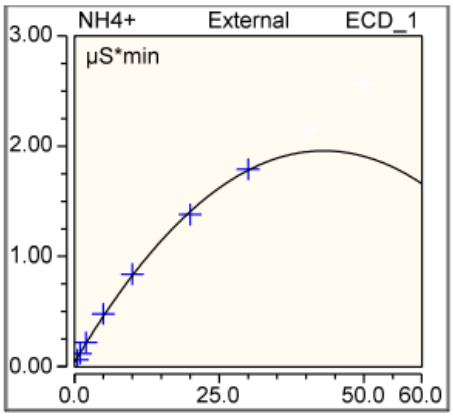

Fig. S6 The standard curves of (a, b) indophenol bule, (c, d) Nessler's reagent, and (e) ion chromatography for ammonium ion concentration detection.

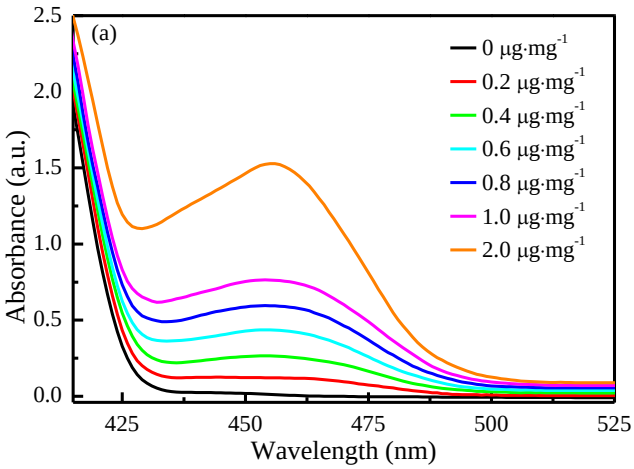

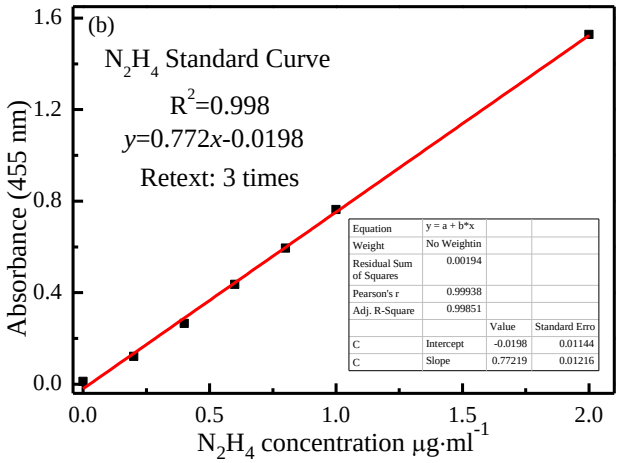

Fig. S7 (a) The UV-Vis absorption spectra and (b) corresponding calibration curves for the colorimetric N_2H_4 assay using the in 0.001 M H_2SO_4.

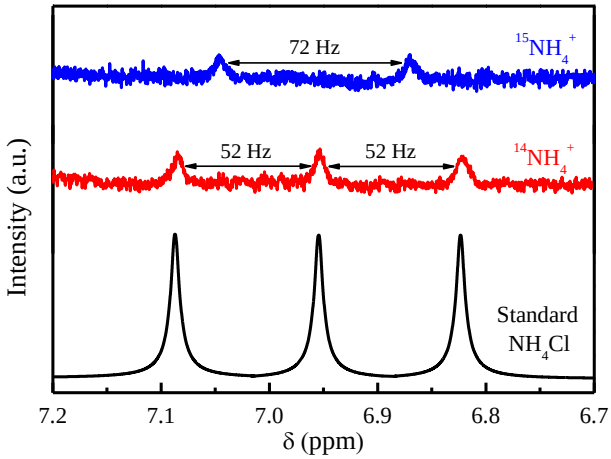

Fig. S8 ^{1}H-NMR (400 MHz) spectra of solution after photocatalytic N_2 fixation through TiCeOS as a photocatalyst in $^{14}N_2$ or $^{15}N_2$ atmosphere.

Table S2 Crystallinity, crystal size, S_{BET}, and XPS analyses of TiO_2, TiOS, and TiCeOS catalysts

Catalyst	Elements percentage (%)				O_V/ O_L+O_V	Ce^{3+}/ Ce^{3+}+ Ce^{4+} (%)	Crystallinity (%)	Crystal size (nm)	S_{BET} (m^2/g)
	Ti	Ce	O	S					
TiO_2	34.18	--	65.82	--	--	--	86.11	5.10	119.28
TiOS	33.76	--	62.59	3.65	4.63	--	82.66	4.30	130.54
TiCeO	31.89	3.86	64.25	--	1.03	2.48	83.52	5.02	123.63
TiCeOS-1	31.96	4.03	59.83	4.18	7.48	18.46	80.92	4.30	162.43
TiCeOS-2	31.88	4.12	59.48	4.52	13.56	35.64	79.63	4.50	183.35
TiCeOS-3	31.81	4.23	59.04	4.92	22.24	56.89	77.68	4.10	197.68
TiCeOS-4	31.39	4.47	58.79	5.35	11.91	63.58	76.64	4.30	175.31
TiCeOS-3 after reaction	31.82	4.14	59.44	4.60	22.12	57.12	77.72	4.10	196.92

Table S3 Element analyses tested by XRF

Catalyst	Ti (%)	Ce (%)	O (%)	S (%)
TiO_2	34.43	--	65.57	--
TiOS	34.03	--	62.50	3.47
TiCeO	32.26	3.92	63.82	--
TiCeOS-1	32.04	4.06	59.81	4.09
TiCeOS-2	31.91	4.16	59.51	4.42
TiCeOS-3	31.85	4.25	59.02	4.88
TiCeOS-4	31.47	4.54	58.69	5.30
TiCeOS-3 after reaction	31.94	4.20	59.50	4.36

Table S4 Element analyses tested by SEM-EDX

Catalyst	Ti (%)	Ce (%)	O (%)	S (%)
TiO_2	35.76	--	64.24	--
TiOS	34.68	--	62.04	3.28
TiCeO	32.58	4.26	63.16	--
TiCeOS-1	32.23	4.33	59.48	3.96
TiCeOS-2	32.11	4.49	59.18	4.22
TiCeOS-3	31.92	4.65	58.57	4.86
TiCeOS-4	31.26	4.82	58.48	5.44
TiCeOS-3 after reaction	32.15	4.48	59.10	4.25

Table S5 The testing results via indophenol blue, Nessler's reagent, and ion chromatography methods

Catalysts	indophenol blue ($\mu mol \cdot g^{-1} \cdot h^{-1}$)	Nessler's reagent ($\mu mol \cdot g^{-1} \cdot h^{-1}$)	ion chromatography ($\mu mol \cdot g^{-1} \cdot h^{-1}$)
TiOS	60.3	68.8	56.0
TiCeOS-1	126.8	133.2	122.5
TiCeOS-2	257.5	262.5	251.8
TiCeOS-3	382.4	395.9	378.1
TiCeOS-4	215.1	220.3	211.7

Table S6 The literature-reported catalysts for photocatalytic N_2 fixation

Photocatalyst	Light source	Reaction medium	Sacrificial agent	NH_3 evolved $\mu mol \cdot g^{-1} \cdot h^{-1}$	NH_3 analysis methods	AQE and STA conversion efficiency	Ref.
CeO_2-$BiFeO_3$	UV−vis	Water	none	117.77 $\mu mol \cdot g^{-1} \cdot h^{-1}$	Nessler's reagent method	--	[10]
TiO_2/$SrTiO_3$/g-C_3N_4	Simulated solar light	Water, ethanol (10%, v/v)	ethanol	2192.0 $\mu mol \cdot g^{-1} \cdot h^{-1}$	Nessler's reagent method	--	[11]
Ag-$KNbO_3$	Simulated solar light	Water, ethanol (10%, v/v)	ethanol	385.0 $\mu mol \cdot g^{-1} \cdot h^{-1}$	Nessler's reagent method	--	[12]
Cu-doped TiO_2	300 W Xe lamp	Water	none	78.90 $\mu mol \cdot g^{-1} \cdot h^{-1}$	Nessler's reagent method and ion chromatography	AQE= 0.74% at 380 nm STA= 0.23% at 420 nm	[13]
Bi-Bi_2WO_6	Simulated solar light	Water	none	86.0 $\mu mol \cdot g^{-1} \cdot h^{-1}$	Nessler's reagent method	--	[14]
Au/TiO2	300 W Xe lamp (λ> 420 nm)	Water, methanol (10%, v/v)	methanol	78.60 $\mu mol \cdot g^{-1} \cdot h^{-1}$	Indophenol-blue method	AQE= 0.82% at 550 nm	[15]
P-doped g-C_3N_4	2 kW Xe lamp (λ> 420 nm)	Water	none	0.20 $\mu mol \cdot h^{-1}$	Ion chromatography	STA= 0.1%	[2]
S-doped g-C_3N_4	500 W Xe lamp	Water, methanol (4%, v/v)	methanol	5990 $\mu mol \cdot g^{-1} \cdot h^{-1}$	Nessler's reagent method	--	[16]
WO_3/CdS	300 W Xe lamp	Water	none	35.8 $\mu mol \cdot g^{-1} \cdot h^{-1}$	ion chromatography	--	[17]
La/MoO_{3-x}	300 W Xe lamp	Water	none	209 $\mu mol \cdot g^{-1} \cdot h^{-1}$	ion chromatography	--	[18]
AgPt–TiO_2	300 W Xe lamp	Water	none	38.4 $\mu mol \cdot g^{-1} \cdot h^{-1}$	ion chromatography	--	[19]
Pt/N–MoS_2	300 W Xe lamp	Water, methanol (10%, v/v)	methanol	133.8 $\mu mol \cdot g^{-1} \cdot h^{-1}$	Nessler's reagent method	--	[20]
F-Vo-TiO_2	300 W Xe lamp	Water	none	206 $\mu mol \cdot g^{-1} \cdot h^{-1}$	ion chromatography	AQE=0.38% at 420 nm	[21]
Reduced TiO_2	300 W Xe lamp	Water, methanol (10%, v/v)	methanol	324.86 $\mu mol \cdot g^{-1} \cdot h^{-1}$	Ion chromatography	AQY=1.1% at 365 nm	[22]
Sb/TiO2	300 W Xe lamp	Water	none	32.2 $\mu mol \cdot g^{-1} \cdot h^{-1}$	Indophenol blue method	--	[23]
TiCeOS-3	300 W Xe lamp (λ> 420 nm)	Water	none	382.4 $\mu mol \cdot g^{-1} \cdot h^{-1}$	Nessler's reagent Method, indophenol blue method, and ion chromatography	AQE= 3.32% at 420 nm STA= 0.058% at AM1.5G	This work

References

[1] X. Chen, X. Zhang, Y. Li, M. Qi, J. Li, Z. Tang, Z. Zhou, Y. Xu, Transition metal doping BiOBr nanosheets with oxygen vacancy and exposed {102} facets for visible light nitrogen fixation, *Appl. Catal. B-Environ.*, 281 (2021) 119516.

[2] Y. Shiraishi, S. Shiota, Y. Kofuji, M. Hashimoto, K. Chishiro, H. Hirakawa, S. Tanaka, S. Ichikawa, T. Hirai, Nitrogen fixation with water on carbon-nitride-based metal-free photocatalysts with 0.1% Solar-to-Ammonia energy conversion efficiency. *ACS Appl. Energy Mater.*, 1 (2018) 4169-4177.

[3] Z. Chen, T.F. Jaramillo, T.G. Deutsch, A. Kleiman-Shwarsctein, A.J. Forman, N. Gaillard, R. Garland, K. Takanabe, C. Heske, M. Sunkara, E.W. McFarland, K. Domen, E.L. Miller, J.A. Turner, H.N. Dinh, Accelerating materials development for photoelectrochemical hydrogen production: Standards for methods, definitions, and reporting protocols, *J. Mater. Res.*, 25 (2010) 3-16.

[4] K. Chen, X. Xu, Q. Mei, J. Huang, G. Yang, Q. Wang, Porous $TiWO_3/SrWO_4$ with high titanium molar ratio for efficient photoelectrocatalytic nitrogen reduction under mild conditions, *Appl. Catal. B-Environ.*, 341 (2024) 123299.

[5] A. Chowdhury, N. Peela, A. Golder, Synthesis of spinel type 2D Co_3O_4 nanodiscs using gallic acid for electrochemical NH_3 formation by N_2 reduction, *Mater. Sci. Eng. B.*, 299 (2024) 116912.

[6] H. Zhao, J. Duan, Z. Zhang, W. Wang, High-performance gas-liquid-solid optofluidic microreactor with TiO_{2-x}-Ag@HKUST-1/carbon paper for efficient photocatalytic nitrogen fixation to ammonia, *Colloids Surf. A: Physicochem. Eng. Aspects.*, 660 (2023) 130874.

[7] D. Wu, J. Tian, Y. Xing, X. Jin, G. Ni, Fabrication of Z-scheme ZnO/Bi_2O_4 heterojunction

photocatalyst with superior photocatalytic nitrogen fixation under visible light irradiation, *Solid State Sci.*, 119 (2021) 106709.

[8] M. Sharma, A. Kumar, D. Gill, S. Jaiswal, A. Patra, S. Bhattacharya, V. Krishnan, Boosting Photocatalytic Nitrogen Fixation via Nanoarchitectonics Using Oxygen Vacancy Regulation in W-Doped Bi_2MoO_6 Nanosheets, *ACS Appl. Mater. Interfaces.*, 15 (2023) 55765-55778.

[9] N. Zhang, A. Jalil, D. Wu, S. Chen, Y. Liu, C. Gao, W. Ye, Z. Qi, H. Ju, C. Wang, X. Wu, L. Song, J. Zhu, Y. Xiong, Refining defect states in $W_{18}O_{49}$ by Mo doping: A strategy for tuning N_2 activation towards solar-driven nitrogen fixation, *J. Am. Chem. Soc.*, 140 (2018) 9434-9443.

[10] S. Mansingh, S. Sultana, R. Acharya, M. Ghosh, K. Parida, Efficient photon conversion via double charge dynamics CeO_2-$BiFeO_3$ p-n heterojunction photocatalyst promising toward N_2 fixation and phenol-Cr (VI) detoxification. *Inorg. Chem.*, 59 (2020) 3856-3873.

[11] R. Tao, X. Li, X. Li, C. Shao, Y. Liu, TiO_2/$SrTiO_3$/g-C_3N_4 Ternary heterojunction nanofibers: Gradient energy band, cascade charge transfer, enhanced photocatalytic hydrogen evolution, and nitrogen fixation. *Nanoscale*, 12 (2020) 8320-8329.

[12] P. Xing, S. Wu, Y. Chen, P. Chen, X. Hu, H. Lin, L.H. Zhao, Y. He, New application and excellent performance of Ag/$KNbO_3$ nanocomposite in photocatalytic NH3 synthesis. *ACS Sustain. Chem. Eng.*, 7 (2019) 12408-12418.

[13] Y. Zhao, Y. Zhao, R. Shi, B. Wang, G.I.N. Waterhouse, L.Z. Wu, C.H. Tung, T. Zhang, Tuning oxygen vacancies in ultrathin TiO_2 nanosheets to boost photocatalytic nitrogen fixation up to 700 nm, *Adv. Mater.*, 31 (2019) 1806482.

[14] S. Zhou, C. Zhang, J. Liu, J. Liao, Y. Kong, Y. Xu, G. Chen, Formation of an priented Bi_2WO_6 photocatalyst induced by in situ bi reduction and its use for efficient nitrogen fixation. *Catal. Sci.*

Technol., 9 (2019) 5562-5566.

[15] J. Yang, Y. Guo, R. Jiang, F. Qin, H. Zhang, W. Lu, J. Wang, J.C. Yu, High-efficiency "workingin tandem" nitrogen photofixation achieved by assembling plasmonic gold nanocrystals on ultrathin titania nanosheets, *J. Am. Chem. Soc.*, 140 (2018) 8497.

[16] S. Cao, B. Fan, Y. Feng, H. Chen, F. Jiang, X. Wang, Sulfur-doped g-C_3N_4 nanosheets with surface carbon vacancies: General synthesis and improved activity for simulated solar-light photocatalytic nitrogen fixation, *Chem. Eng. J.*, 353 (2018) 147-156.

[17] P. Xia, X. Pan, S. Jiang, J. Yu, B, He, P.M. Ismail, W. Bai, J. Yang, H. Zhang, M. Cheng, H. Li, Q. Zhang, C. Xiao, Y. Xie, Designing a redox heterojunction for photocatalytic "overall nitrogen fixation" under mild conditions. *Adv, Mater.*, 34 (2022) 2200563.

[18] X. Liu, Y. Luo, C. Ling, Y. Shi, G. Zhan, H. Li, H. Gu, K. Wei, F. Guo, Z. Ai, L. Zhang, Rare earth La single atoms supported MoO_{3-x} for efficient photocatalytic nitrogen fixation. *Appl. Catal. B. Environ.*, 301 (2022) 120766.

[19] X. Bian, Y. Zhao, S. Zhang, D. Li, R. Shi, C. Zhou, L.Z. Wu, T. Zhang, Enhancing the supply of activated hydrogen to promote photocatalytic nitrogen fixation. *ACS Mater. Lett.*, 3 (2021) 1521-1527.

[20] H. Maimaitizi, A. Abulizi, T. Zhang, K. Okitsu, J. Zhu, Facile photo-ultrasonic assisted synthesis of flower-like Pt/N-MoS_2 microsphere as an efficient sonophotocatalyst for nitrogen fixation. *Ultrason. Sonochem.*, 63 (2020) 104956.

[21] R. Guan, D. Wang, Y. Zhang, C. Liu, W. Xu, J. Wang, Z. Zhao, M. Feng, Q. Shang, Z. Sun, Enhanced photocatalytic N_2 fixation via defective and fluoride modified TiO_2 surface, *Appl. Catal. B: Environ.*, 282 (2021) 119580.

[22] G. Zhang, X.Yang, C. He, P. Zhang, H. Mi, Constructing a tunable defect structure in TiO_2 for photocatalytic nitrogen fixation. *J. Mater. Chem. A.*, 8 (2020) 334-341.

[23] Z. Zhao, S. Hong, C. Yan, C. Choi, Y. Jung, Y. Liu, S. Liu, X. Li, J. Qiu, Z. Sun, Efficient visible-light driven N_2 fixation over two-dimensional Sb/TiO_2 composites. *Chem. Comm.*, 55 (2019) 7171-7174.